

Image-based localization using LSTMs for structured feature correlation

F. Walch¹ C. Hazirbas¹ L. Leal-Taixé¹ T. Sattler² S. Hilsenbeck³ D. Cremers¹

¹Technical University Munich ²ETH Zürich ³NavVis

Abstract

In this work we propose a new CNN+LSTM architecture for camera pose regression for indoor and outdoor scenes. CNNs allow us to learn suitable feature representations for localization that are robust against motion blur and illumination changes. We make use of LSTM units on the CNN output, which play the role of a structured dimensionality reduction on the feature vector, leading to drastic improvements in localization performance. We provide extensive quantitative comparison of CNN-based vs SIFT-based localization methods, showing the weaknesses and strengths of each. Furthermore, we present a new large-scale indoor dataset with accurate ground truth from a laser scanner. Experimental results on both indoor and outdoor public datasets show our method outperforms existing deep architectures, and can localize images in hard conditions, e.g., in the presence of mostly textureless surfaces.

1. Introduction

Being able to localize a vehicle or device by estimating a camera pose from an image is a fundamental requirement for many computer vision applications such as navigating autonomous vehicles [31], mobile robotics and Augmented Reality [33], and Structure-from-Motion (SfM) [42].

Most state-of-the-art approaches [28, 41, 46, 58] rely on local features such as SIFT [32] to solve the problem of image-based localization. Given a SfM model of a scene, where each 3D point is associated with the image features from which it was triangulated, one proceeds in two stages [29, 40]: (i) establishing 2D-3D matches between features extracted from the query image and 3D points in the SfM model via descriptor matching; (ii) using these correspondences to determine the camera pose, usually by employing a n -point solver [26] for pose estimation inside a RANSAC loop [11]. Obviously, pose estimation can only succeed if enough correct matches have been found in the first stage. Consequently, limitations of both the feature detector, *e.g.*, motion blur or strong illumination changes, or the descrip-



(a) PoseNet result [22]

(b) Our result

Figure 1: Accurate outdoor image-based localization achieved by the proposed method, even in challenging lighting conditions where other deep architectures fail.

tor, *e.g.*, due to strong viewpoint changes, will cause localization approaches to fail.

In recent literature, two approaches have tackled the problem of localization with end-to-end learning. PlaNet [53] formulates localization as a classification problem, where the current position is matched to the best position in the training set. While this approach is suitable for localization in extremely large environments, it only allows to recover position but not orientation and its accuracy is bounded by the spatial extent of the training samples. More similar in spirit to our approach, PoseNet [21, 22] formulates 6DoF pose estimation as a regression problem, but its performance is still far below state-of-the-art SIFT methods [28, 41, 46, 58].

1.1. Contribution

In this paper, we propose to directly regress the camera pose from an input image. To do so, we leverage, on the one hand, Convolutional Neural Networks (CNNs) which allow us to learn suitable feature representations for localization that are more robust against motion blur and illumination changes. As we can see from the PoseNet [22] results, regressing the pose after the high dimension output of a fully connected (FC) layer is not optimal. Our intuition is that the high dimension of the FC output makes the network prone overfitting to training data. PoseNet deals with this problem with careful dropout strategies. We propose to make use of Long-Short Term Memory (LSTM) units on the FC output,

which performs structured dimensionality reduction, choosing the most useful feature correlations for the task of pose estimation. Overall, we improve localization accuracy by 32-38% wrt previous deep learning architectures [22]. Furthermore, we provide an extensive comparison with state-of-the-art SIFT-based methods, which shreds a light on the strengths and weaknesses of each approach. Finally, we introduce a new dataset for large-scale indoor localization, consisting of more than 3,330 high resolution images covering a total area of 9,225 square meters. Each image contains geo-referenced pose information. This dataset is specially challenging for SIFT-based methods, as it contains large textureless areas and repetitive structures. We show that our approach is robust also in these scenarios, and is able to localize images on average within 1m of their ground truth location.

To summarize, our contribution is three-fold:

- We propose a new CNN+LSTM architecture for camera pose regression that works in indoor and outdoor scenes.
- We provide an extensive quantitative comparison of CNN-based vs SIFT-based localization methods.
- We introduce a new challenging large indoor benchmark with accurate ground truth pose information.

1.2. Related work

Local feature-based localization. There are two traditional ways to approach the localization problem. Location recognition methods represent a scene by a database of geo-tagged photos. Given a query image, they employ image retrieval techniques to identify the database photo most similar to the query [2, 39, 48, 49, 57]. The geo-tag of the retrieved image is often used to approximate the camera pose of the query, even though a more accurate estimate can be obtain by retrieving multiple relevant images [56, 59].

More relevant to our approach are structure-based localization techniques that use a 3D model, usually obtained from Structure-from-Motion, to represent a scene. They determine the full 6DoF camera pose of a query photo from a set of 2D-3D correspondences established via matching features found in the query against descriptors associated with the 3D points. The computational complexity of matching grows with the size of the model. Thus, prioritized search approaches [8, 29, 41] terminate correspondence search as soon as a fixed number of matches has been found. Similarly, descriptor matching can be accelerated by using only a subset of all 3D points [7, 29], which at the same time reduces the memory footprint of the 3D models. The latter can also be achieved by quantizing the descriptors [33, 38].

For more complex scenes, e.g., large-scale urban environments or even large collections of landmark scenes, 2D-3D matches are usually less unique as there often are multiple 3D points with similar local appearance [28]. This causes problems for the pose estimation stage as accepting more matches leads to more wrong matches and RANSAC’s run-time grows exponentially with the ratio of wrong matches. Consequently, Sattler *et al.* use co-visibility information between 3D points to filter out wrong matches before pose estimation [38, 41]. Similarly, Li *et al.* use co-visibility information to adapt RANSAC’s sampling strategy, enabling them to avoid drawing samples unlikely to lead to a correct pose estimate [28]. Assuming that the gravity direction and a rough prior on the camera’s height are known, Svärm *et al.* propose an outlier filtering step whose run-time does not depend on the inlier ratio [46]. Zeisl *et al.* adapt their approach into a voting scheme, reducing the computational complexity of outlier filtering from $\mathcal{O}(n^2 \log n)$ [46] to $\mathcal{O}(n)$ for n matches [58].

The overall run-time of classical localization approaches depends on the number of features found in a query image, the number of 3D points in the model, and the number of found correspondences and/or the percentage of correct matches. In contrast, our approach directly regresses the camera pose from a single feed-forward pass through a network. As such, the run-time of our approach only depends on the size of the network used.

As we will show, SIFT-based methods do not work for our new challenging indoor LSI dataset due to repetitive structures and large textureless regions present in indoor scenes. This further motivates the use alternative approaches based e.g. on deep learning.

Localization utilizing machine learning. In order to boost location recognition performance, Gronat *et al.* and Cao & Snavely learn linear classifiers on top of a standard bag-of-words representation [6, 16]. They divide the database images into distinct places and train the classifiers to distinguish between them.

Donoser and Schmalstieg cast feature matching as a classification problem, where the descriptors associated with each 3D model point form a single class [10]. They employ an ensemble of random ferns to compute correspondences, which enable fast run-times. Still, descriptor matching-based approaches are able to localize more images.

Aubry *et al.* learn feature descriptors specifically for the task of localizing paintings against 3D scene models [3].

In the context of re-localization for RGB-D images, Guzman-Rivera *et al.* and Shotton *et al.* learn random forests that predict a 3D point position for each pixel in an image [17, 43]. The resulting 2D-3D matches are then used to estimate the camera pose using RANSAC. Rather than predicting point correspondences, Valentin *et al.* explicitly model the uncertainty of the predicted 3D point positions

and use this uncertainty during pose estimation [50], allowing them to localize more images. Brachmann *et al.* adapt the random forest-based approach to not rely on depth measurements during test time such that RGB-only images can be localized as well [4]. Still, they require depth data during the training stage as to predict 3D coordinates for each pixel. In contrast to these methods, our approach directly regresses the camera pose from an RGB image, and thus only needs a set of image-pose pairs as input for training.

Deep learning. CNNs have been successfully applied to most tasks in computer vision since their major success in image classification [19, 25, 44] and object detection [12, 13, 36]. One of the major drawbacks of deep learning is its need for large datasets for training. A common approach used for many tasks is that to fine-tune deep architectures pre-trained on the seemingly unrelated task of image classification on ImageNet [37]. This has been successfully applied to object detection [12], object segmentation [24, 34], semantic segmentation [18, 35], depth and normal estimation [27], to name a few. Similarly, we take pre-trained networks, *e.g.* GoogLeNet [47], which can be seen as feature extractors and are then fine-tuned for the task of camera pose regression.

LSTM [20] is a type of Recurrent Neural Network (RNN) [14] designed to accumulate or forget relevant contextual information in its hidden state. It has been successfully applied for handwriting recognition [15] or in natural language processing for machine translation [45]. Recently, CNN and LSTM have been combined in the computer vision community to tackle, for example, visual recognition in videos [9]. While most methods in the literature apply LSTM on a temporal sequence, recent works have started to use the memory capabilities of LSTMs to encode contextual information. ReNet [52] replaced convolutions by RNNs sweeping the image vertically and horizontally. [51] uses spatial LSTM for person re-identification, parsing the detection bounding box horizontally and vertically in order to capture spatial dependencies between body parts. [5] employs the same idea for semantic segmentation, and [30] for semantic object parsing. We use LSTMs to better correlate features coming out of the convolutional and FC layers, efficiently reducing feature dimensionality in a structured way that improves pose estimation compared to using dropout on the feature vector to prevent overfitting.

End-to-end learning has also been used for localization and location recognition. Arandjelović *et al.* employ CNNs to learn compact image representations, where each image in a database is represented by a single descriptor [1]. Weyand *et al.* cast localization as a classification problem [53]. They adaptively subdivide the earth’s surface in a set of tiles, where a finer quantization is used for regions exhibiting more images. The CNN then learns to predict the corresponding tile for a given image, thus providing the ap-

proximate position from which a photo was taken. Focusing on accurate 6DoF camera pose estimation, the PoseNet method by Kendall *et al.* uses CNNs to model pose estimation as a regression problem [22]. An extension of the approach repeatedly evaluates the CNN with a fraction of its neurons randomly disabled, resulting in multiple different pose predictions that can be used to predict pose uncertainty [21]. One drawback of the PoseNet approach is its relative inaccuracy [4]. In this paper, we show how a CNN+LSTM architecture is able to produce significantly more accurate camera poses.

2. Deep camera pose regression

In this section we develop our framework for learning to regress camera poses directly from images. Our goal is to train a CNN+LSTM network to learn a mapping from an image to a pose, $I \xrightarrow{f} \mathbf{P}$, where $f(\cdot)$ is the neural network. Each pose $\mathbf{P} = [\mathbf{p}, \mathbf{q}]$ is represented by its 3D camera position $\mathbf{p} \in \mathbb{R}^3$ and a quaternion $\mathbf{q} \in \mathbb{R}^4$ for its orientation.

Given a dataset composed of training images I_i and their corresponding 3D ground truth poses \mathbf{P}_i , we train the network using Adam [23] with the following loss function:

$$L_i = \|\mathbf{p}_i - \hat{\mathbf{p}}_i\|_2 + \beta \cdot \left\| \mathbf{q}_i - \frac{\hat{\mathbf{q}}_i}{\|\hat{\mathbf{q}}_i\|} \right\|_2 \quad (1)$$

where (\mathbf{p}, \mathbf{q}) and $(\hat{\mathbf{p}}, \hat{\mathbf{q}})$ are ground truth and estimated position-orientation pairs, respectively. We represent the orientation with quaternions and thus normalize the predicted orientation $\hat{\mathbf{q}}_i$ to unit length. β determines the relative weight of orientation error to positional error and is in general bigger for outdoor scenes, as errors tend to be relatively larger. All hyperparameters used for the experiments are detailed in Section 4.

2.1. CNN architecture: feature extraction

Training a neural network from scratch for the task of pose regression would be impractical for several reasons: (i) we would need a really large training set, (ii) compared to classification problems, where each output label is covered by at least one training sample, the output in regression is continuous and infinite. Therefore, we leverage a pre-trained classification network, namely GoogLeNet [47], and modify it in a similar fashion as [22]. At the end of the convolutional layers average pooling is performed, followed by a fully connected layer which outputs a 2048 dimensional vector, see Figure 2. This can be seen as a feature vector that represents the image to be localized. This architecture is directly used by [22] to predict camera poses, by using yet another fully connected regression layer at the end that outputs the 7-dimensional pose and orientation vector (the quaternion vector is normalized to unit length at test time).

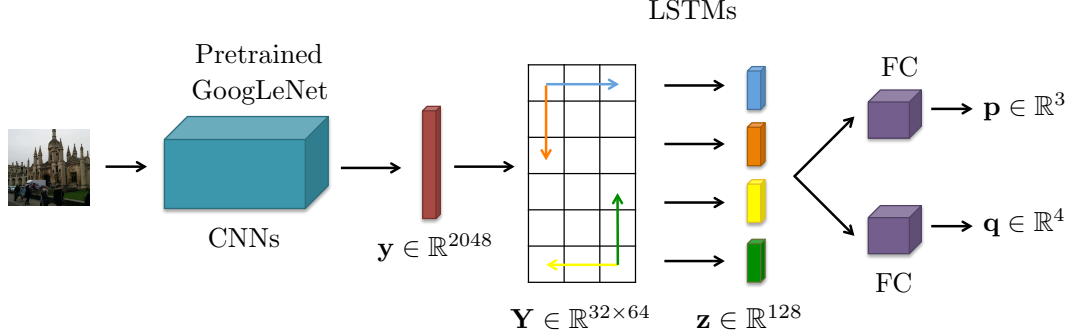


Figure 2: Architecture of the proposed pose regression LSTM network.

2.2. Structured feature correlation with LSTMs

After the convolutional layers of GoogleNet, an average pooling layer gathers the information of each feature channel for the entire image. Following PoseNet [22], we use a fully connected (FC) layer after pooling to learn the correlation among features. As we can see from the PoseNet [22] results, regressing the pose after the high dimension output of a fully connected (FC) layer is not optimal. Our intuition is that the high dimension of the FC output makes the network prone overfitting to training data. Dropout helps reduce this effect in PoseNet. One could also reduce the feature dimension of the FC, but we empirically found that dimensionality reduction performed by the network with memory blocks is more efficient than hand-crafting it.

Even though Long Short-Term Memory (LSTM) units have been typically applied to temporal sequences, recent works [5, 30, 51, 52] have used the memory capabilities of LSTMs in image space. In our case, we treat the output 2048 feature vector as our sequence. We propose to insert four LSTM units after the FC, which have the function of reducing the dimensionality of the feature vector in a structured way. The memory units filter out the most useful feature correlations for the task of pose estimation.

Reshaping the input vector. In practice, inputting the 2048-D vector directly to the LSTM did not show good results. Intuitively, this is because even though the memory unit of the LSTM is capable of remembering distant features, a 2048 length vector is too long for LSTM to correlate from the first to the last feature. We thereby propose to reshape the vector to a 32×64 matrix, and to apply four LSTMs in the up, down, left and right directions as depicted in Figure 2. These four outputs are then concatenated and passed to the fully connected pose prediction layers. This imitates the function of structured dimensionality reduction which greatly improves pose estimation results.

3. Large-scale indoor localization dataset

Machine learning and in particular deep learning are inherently data-intensive endeavors. Specifically, supervised

learning requires not only data but also associated ground truth labelling, often the hardest to achieve. For some tasks such as image classification [37] or outdoor image-based localization [22] large training and testing datasets have already been made available to the community. For indoor scenes, only small datasets covering a spatial extent the size of a room [43] are currently available. The lack of extensive data collections either results in unrealistic training prone to overfitting, or makes researchers resort to their own non-public data, making it difficult to compare contributions.

We introduce *LSI Localization Dataset*, a new large-scale indoor (LSI) localization image collection covering an area two orders of magnitude larger than 7Scenes [43]. LSI Localization Dataset comprises 3,330 high-resolution images (4592×3448) with geo-referenced pose information for each image. Organized in three sequences, the dataset spans two connected buildings across a city university campus, covering a total indoor area of 9225 square meters. Image locations are spaced roughly one meter apart and at each, we provide a set of six wide-angle pictures, taken in five different horizontal directions (full 360°) and one pointing up (see Figure 3). The depicted buildings feature multiple architectural styles with numerous variations of appearance and geometry, ranging from ornamental mosaic floors to modern plain concrete.

In order to generate ground truth pose information for each image, we captured the data using the *NavVis M3*¹ indoor mapping platform. This mobile system is equipped with six *Panasonic* 16-Megapixel system cameras and three *Hokuyo* laser range finders. Employing SLAM, the platform is able to reconstruct the full trajectory with sub-centimeter accuracy while being pushed through an indoor environment. We captured the various buildings and floor levels in multiple sequences which we manually aligned with respect to each other as well as to the global coordinate frame.

¹www.navvis.com

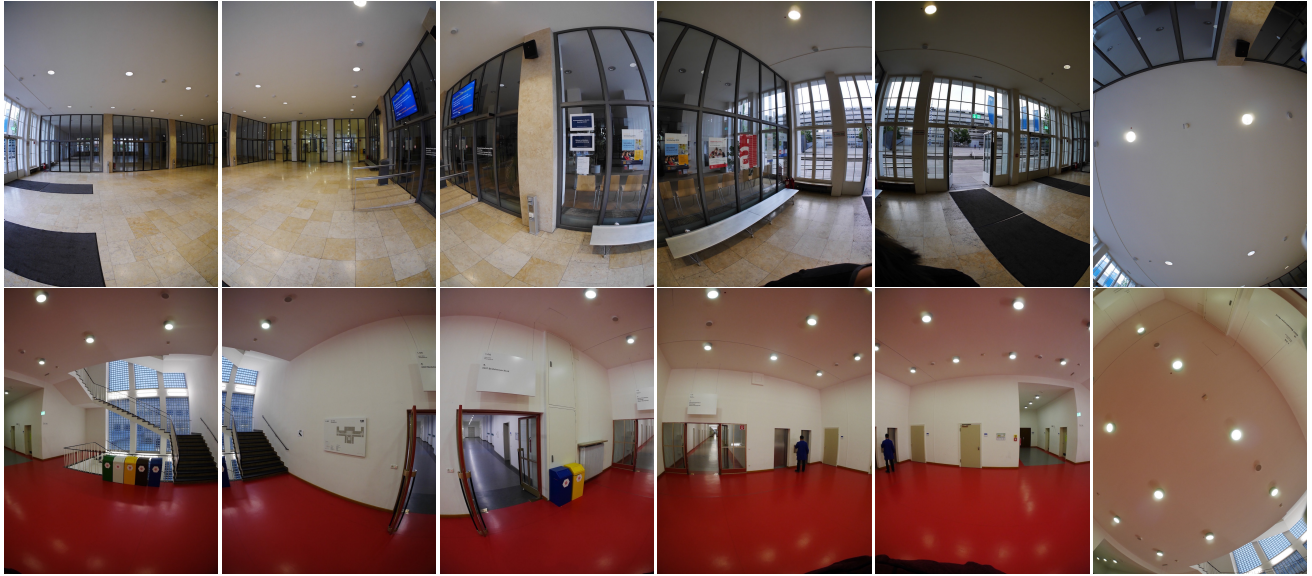


Figure 3: Example images from our LSI Localization Dataset. At each capture-location, we provide a set of six high-resolution wide-angle pictures, taken in five different horizontal directions and one pointing up.

4. Experimental results

We present results on several datasets, proving the efficacy of our method in outdoor scenes like Cambridge [22] and small-scale indoor scenes such as 7Scenes [43]. The two datasets are very different from each other: 7Scenes has a very high number of images in a very small spatial extent, hence, it is more suited for applications such as Augmented Reality, while Cambridge Landmarks has sparser coverage and larger spatial extent, the perfect scenario for image-based localization. In the experiments, we show our method can be applied to both scenarios delivering competitive results. We provide comparisons to previous CNN-based approaches, as well as a state-of-the-art SIFT-based localization method. Furthermore, we provide results for our new large-scale indoor LSI Localization dataset. SIFT-based methods fail on these sequences due to textureless surfaces and repetitive structures, while our method is able to localize images with an average accuracy of 1.30m for an area of 9,225 square meters.

Experimental setup. We initialize the GoogLeNet part of the network with the Places [60] weights and randomly initialize the remaining weights. All networks take images of size 224×224 pixel as input. We use random crops during training and central crops during testing. A mean image is computed separately for each training sequence and is subtracted from all images. All experiments are performed on an NVIDIA Titan X using TensorFlow with Adam [23] for optimization. Random shuffling is performed for each batch, and regularization is only applied to weights, not biases. For all sequences we use the following hyperparam-

eters: batch size 75, regularization $\lambda = 2^{-4}$, auxiliary loss weights $\gamma = 0.3$, dropout probability 0.5, and the parameters for Adam: $\epsilon = 1$, $\beta_1 = 0.9$ and $\beta_2 = 0.999$. The β of Eq. 1 balances the orientation and positional penalties. To ensure a fair comparison, for Cambridge Landmarks and 7Scenes, we take the same values as PoseNet [22]: for the indoor scenes β is between 120 to 750 and outdoor scenes between 250 to 2000. For the LSI Localization dataset, we set $\beta = 1000$.

Comparison with state-of-the-art. We compare results to two CNN-based approaches: PoseNet [22] and Bayesian PoseNet [21]. On Cambridge Landmarks and 7Scenes, results for the two PoseNet variants [21, 22] were taken directly from the author’s publication [21]. For the new LSI Localization dataset, their model was fine-tuned with the training images. The hyperparameters used are the same as for our method, except for Adam parameter $\epsilon = 0.1$, which showed better convergence.

To the best of our knowledge, CNN-based approaches have not been quantitatively compared to SIFT-based localization approaches. We feel this comparison is extremely important to know how deep learning can make an impact in image-based localization, and what challenges are there to overcome. We therefore present results of a state-of-the-art SIFT-based method, namely Active Search [41].

Active Search estimates the camera poses wrt a SfM model, where each 3D point is associated with SIFT descriptors extracted from the training images. Since none of the datasets provides both an SfM model and the SIFT descriptors, we constructed such models from scratch using

Table 1: Median localization results of several RGB-only methods on Cambridge Landmarks [22] and 7 Scenes [43].

Scene	Area or Volume	Active Search (w/o) [41]	Active Search (w/) [41]	PoseNet [22]	Bayesian PoseNet [21]	Proposed
King's College	$5600 m^2$	0.59 m, 0.48° (0)	0.67 m, 0.52° (0)	1.92 m, 5.40°	1.74 m, 4.06°	0.99 m, 3.65°
Old Hospital	$2000 m^2$	1.25 m, 0.71° (5)	1.29 m, 0.79° (8)	2.31 m, 5.38°	2.57 m, 5.14°	1.51 m, 4.29°
Shop Façade	$875 m^2$	0.18 m, 0.65° (0)	0.17 m, 0.53° (1)	1.46 m, 8.08°	1.25 m, 7.54°	1.18 m, 7.44°
St Mary's Church	$4800 m^2$	0.26 m, 0.50° (1)	0.29 m, 0.55° (1)	2.65 m, 8.48°	2.11 m, 8.38°	1.52 m, 6.68°
Average All	–	–	–	2.08 m, 6.83°	1.92 m, 6.28°	1.30 m, 5.52°
Average by [41]	–	0.57 m, 0.59°	0.61 m, 0.60°	–	–	1.37 m, 5.52°
<hr/>						
Chess	$6 m^3$	0.04 m, 1.96° (0)	0.04 m, 2.02° (0)	0.32 m, 8.12°	0.37 m, 7.24°	0.24 m, 5.77°
Fire	$2.5 m^3$	0.03 m, 1.93° (1)	0.03 m, 2.02° (1)	0.47 m, 14.4°	0.43 m, 13.7°	0.34 m, 11.9°
Heads	$1 m^3$	0.03 m, 2.59° (7)	0.03 m, 2.77° (8)	0.29 m, 12.0°	0.31 m, 12.0°	0.21 m, 13.7°
Office	$7.5 m^3$	0.09 m, 3.61° (34)	0.10 m, 3.80° (34)	0.48 m, 7.68°	0.48 m, 8.04°	0.30 m, 8.08°
Pumpkin	$5 m^3$	0.08 m, 3.10° (71)	0.09 m, 3.21° (68)	0.47 m, 8.42°	0.61 m, 7.08°	0.33 m, 7.00°
Red Kitchen	$18 m^3$	0.07 m, 3.37° (0)	0.07 m, 3.52° (0)	0.59 m, 8.64°	0.58 m, 7.54°	0.37 m, 8.83°
Stairs	$7.5 m^3$	not available	not available	0.47 m, 13.8°	0.48 m, 13.1°	0.40 m, 13.7°
Average All	–	–	–	0.44 m, 10.4°	0.47 m, 9.81°	0.31 m, 9.85°
Average by [41]	–	0.06 m, 2.76°	0.06 m, 2.89°	–	–	0.30 m, 9.15°

VisualSfM [54, 55] and registered them against the ground truth poses of the training images. The models used for localization do not contain any contribution from the testing images.

Active Search uses a visual vocabulary to accelerate descriptor matching. We trained a vocabulary containing 10k words from training images of the Cambridge dataset and a vocabulary containing 1k words from training images of the smaller 7scenes dataset. Active Search uses these vocabularies for prioritized search for efficient localization, where matching is terminated once a fixed number of correspondences has been found. We report results both with (w/) and without (w/o) prioritization. In the latter case, we simply do not terminate matching early but try to find as many correspondences as possible.

Given a set of 2D-3D matches, Active Search estimates the camera pose via RANSAC [11]. For the Cambridge dataset, we use the known intrinsic calibrations of the testing images while we estimate the intrinsic parameters together with the pose for 7scenes. Poses estimated from only few matches are usually rather inaccurate. Following common practice [28, 29], Active Search only considers a testing image as successfully localized if its pose was estimated from at least 12 inliers.

4.1. Large-scale outdoor localization

We present results for outdoor image-based localization on the publicly available Cambridge Landmarks dataset [22] in Table 1. We report results for Active Search only for images with at least 12 inliers and give the number of images where localization fails in parenthesis. Notice that

the substantially higher error of Active Search on the Old Hospital sequence comes from a less accurate registration of the SfM model. In order to compare the methods fairly, we provide the average accuracy for all images (Average All), and also the average accuracy for only those images that [41] was able to localize (Average by [41]). Note, that we do not report results on the Street dataset of Cambridge Landmarks. It is a unique sequence because the training database consists of four distinct video sequences, each filmed in a different compass direction. This results in training images at similar positions, but with very different orientations. Even with the hyperparameters set by the author of [22], training did not converge for any of the implemented methods.

As we can see, the proposed method reduces positional error by 37.5% wrt CNN-based method PoseNet and the orientation error by 19%. This shows that the proposed LSTM-based structured output is efficient in encoding feature correlations, leading to large improvements in local-



Figure 4: The class activation map is overlaid on an input image from King's College as a heat map. Red areas indicate parts of the image the network considers important for pose regression. The visualization shows how the network focuses on distinctive building elements.

Table 2: Median localization results on scenes from the LSI Localization dataset.

Scene	Area	# train/test	PoseNet [22]	Proposed
Matriculation Hall	793 m ²	940/235	1.15 m, 3.93°	0.85 m, 3.25°
Hallway	2677 m ²	845/215	2.16 m, 6.99°	1.04 m, 4.75°
Floor	5575 m ²	875/220	1.87 m, 6.14°	1.31 m, 2.79°
Average			1.72 m, 5.68°	1.07 m, 3.59°

ization performance. It is important to note that we can still not match the precision of state-of-the-art SIFT-based methods [41], especially when computing the orientation of the camera. Since [41] requires 12 inliers to consider an image as localized, its is able to reject inaccurate poses. In contrast, our method always provides a localization result, even if it is sometimes less accurate. Depending on the application, one behavior or the other might be more desirable. As an example, we show in Figure 5 an image from Old Hospital, where a tree is occluding part of the building. In this case, [41] is not able to localize the image, while our method still produces a reasonably accurate pose. This phenomenon becomes more important in indoor scenes, where Active Search is unable to localize a substantially larger number of images.

Interestingly, for our method, the average for all images is lower than the average only for the images that [41] can also localize. This means that for images where classic methods [41] cannot return a pose, our method actually provides a very accurate result. This “complementary” behavior between SIFT- and CNN-based methods could be exploitable in future research. Overall, our method shows a strong performance in outdoor image-based localization, as seen in Figure 6, where CNN-only method [22] provides less accurate poses. In order to better understand how the network localizes an image, we plot the class activation maps for the King’s College sequence in Figure 4. Notice how strong activations cluster around distinctive building elements, such as the towers or the entrance.

4.2. Small-scale indoor localization

In this section, we focus on localization on small indoor spaces, for which we use the publicly available 7Scenes dataset [43]. Results at the bottom of Table 1 show that we also outperform previous CNN-based PoseNet by 32% in positional error and 5.3% orientation error. There are two methods that use RGB-D data and achieve a lower error: [4] achieves 0.06m positional error and 2.7° orientation error, while [43] scores 0.08m and 1.60°. Note, that these methods require RGB-D data for training [4] and/or testing [43]. In theory, multi-view stereo methods could be used to obtain the required depth maps for outdoor scenes. However, such depth maps are usually substantially more noisy and contain significantly more outliers compared to the data obtained with RGB-D sensors. In addition, the accuracy of

the depth maps decreases quadratically with the distance to the scene, which is usually much larger for outdoor scenes than for indoor scenes. As such, it is unclear how well such methods would work with stereo data.

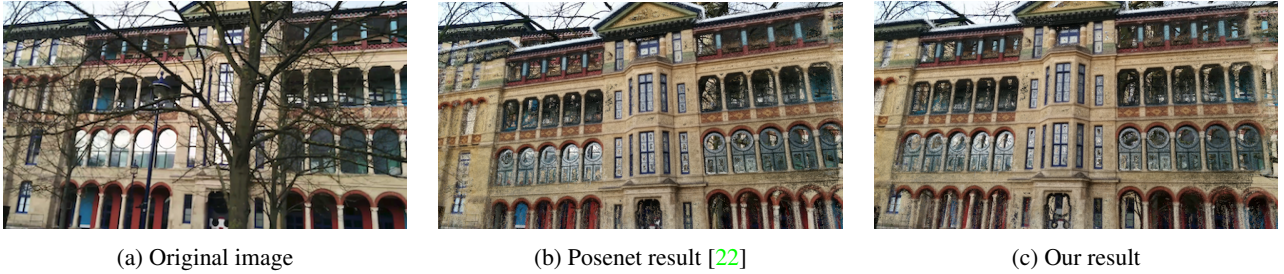
As we can see, Active Search is able to localize images accurately on the indoor scenes. Notice that VisualSfM failed to produce a good reconstruction on the Stairs sequence and we thus cannot evaluate Active Search on this sequence. For the other sequences, the number of images not localized is fairly large, 34 for Office and 71 for Pumpkin. If an image can be localized, we notice that Active Search performs better than CNN-based approaches and comparable² to [4, 43] even though these approaches rely on depth maps for training. We provide the average accuracy for all images (Average All), and also the average accuracy for only those images that [41] was able to localize (Average by [41]). Note that for our method, the two averages are extremely similar, which means that we are able to localize those images with the same accuracy as all the rest, showing robustness wrt textureless surfaces that heavily affect SIFT-based methods. This shows the potential of CNN-based methods.

4.3. Large-scale indoor localization

In our last experiment, we present results on the new LSI Localization dataset. These sequences cover a total area of 9225 square meters, the same order of magnitude as the outdoor localization dataset, and much larger than typical indoor datasets like 7Scenes.

Figure 3 shows an example from the dataset that contains large textureless surfaces. These surfaces are known to cause problems for methods based on local features. In fact, we were not able to obtain correct SfM reconstructions for the LSI Localization dataset, and thus cannot report results for Active Search. The lack of texture in most parts of the images, combined with repetitive scene elements, causes VisualSfM to fold repetitive structures onto themselves. For example, the two separate stairwells (red floor in Figure 3) are mistaken for a single stairwell. Such repetitive structures will cause Active Search to fail even if a good model is provided.

²Notice that part of the localization error for Active Search is caused by registering the SfM reconstructions against the ground truth poses of the training images.

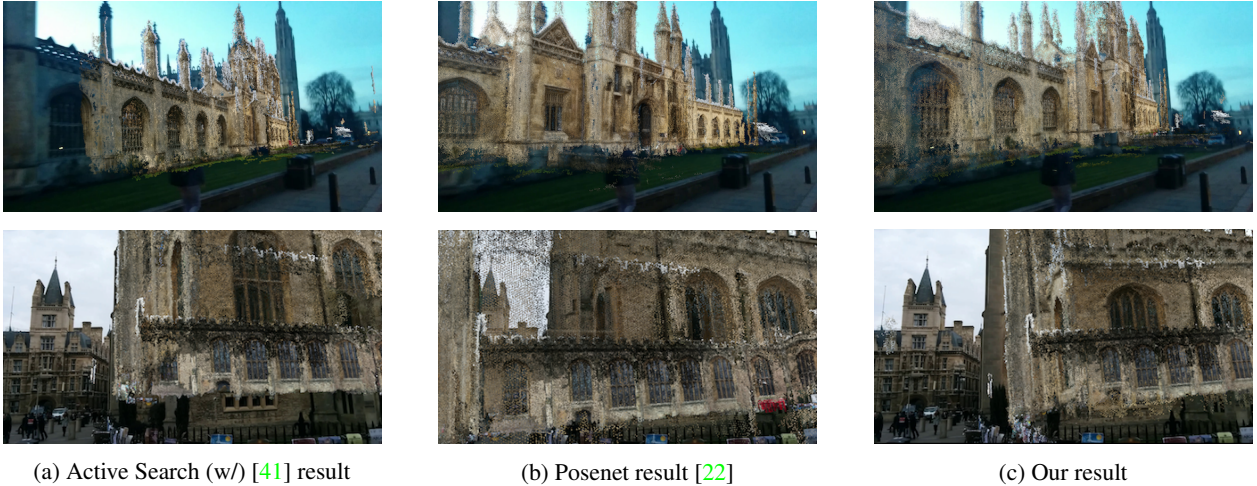


(a) Original image

(b) Posenet result [22]

(c) Our result

Figure 5: Example of the Old Hospital sequence. Resulting 3D model is overlaid according to (b) PoseNet [22] result and (c) our result. Active Search [41] was not able to localize the image due to the occlusion made by the tree. Note the inaccuracy of the PoseNet result compared to the proposed method (check the top of the building for alignment).



(a) Active Search (w/ [41] result

(b) Posenet result [22]

(c) Our result

Figure 6: Examples of localization results on King's College for Active Search [41], PoseNet [22], and the proposed method.

For the experiments on the LSI Localization dataset, we ignore the ceiling-facing cameras. As we can see in Table 2, our method outperforms PoseNet [22] by almost 38% in positional error and 37% orientation error, showing a similar improvement as for other datasets. Most notably, the average error of our method is around 1m on such a large-scale dataset where SIFT-based methods fail. This shows a case where our deep architecture outperforms classic SIFT-based methods and opens up tremendous possibilities for image-based localization in indoor scenes.

5. Conclusion

In this paper, we address the challenge of image-based localization of a camera or an autonomous system with a novel deep learning architecture that combines a CNN with LSTM units. Rather than precomputing feature points and building a map as done in traditional SIFT-based localization techniques, we determine a direct mapping from the input images to a camera pose. Whereas the performance of previous deep learning approaches has remained far below the performance of SIFT-based techniques, we demonstrate that our LSTM-based structured feature correlation can lead

to drastic improvements in localization performance. This is confirmed through a systematic evaluation on several existing data sets. In addition, we introduce a new challenging large indoor dataset with accurate ground truth that cannot be handled with classic SIFT-based methods.

References

- [1] R. Arandjelović, P. Gronat, A. Torii, T. Pajdla, and J. Sivic. NetVLAD: CNN architecture for weakly supervised place recognition. In *CVPR*, 2016. 3
- [2] R. Arandjelović and A. Zisserman. DisLocation: Scalable descriptor distinctiveness for location recognition. In *ACCV*, 2014. 2
- [3] Aubry, Mathieu and Russell, Bryan C. and Sivic, Josef. Painting-to-3D Model Alignment via Discriminative Visual Elements. *ACM TOG*, 33(2):14:1–14:14, 2014. 2
- [4] E. Brachmann, F. Michel, A. Krull, M. Y. Yang, S. Gumhold, and C. Rother. Uncertainty-driven 6d pose estimation of objects and scenes from a single rgb image. In *CVPR*, 2016. 3, 7
- [5] W. Byeon, T. M. Breuel, F. Raue, and M. Liwicki. Scene labeling with lstm recurrent neural networks. In *CVPR*, 2015. 3, 4

[6] S. Cao and N. Snavely. Graph-Based Discriminative Learning for Location Recognition. In *CVPR*, 2013. 2

[7] S. Cao and N. Snavely. Minimal Scene Descriptions from Structure from Motion Models. In *CVPR*, 2014. 2

[8] S. Choudhary and P. J. Narayanan. Visibility probability structure from sfm datasets and applications. In *ECCV*, 2012. 2

[9] J. Donahue, L. A. Hendricks, S. Guadarrama, M. Rohrbach, S. Venugopalan, K. Saenko, and T. Darrell. Long-term recurrent convolutional networks for visual recognition and description. In *CVPR*, 2015. 3

[10] M. Donoser and D. Schmalstieg. Discriminative Feature-to-Point Matching in Image-Based Localization. In *CVPR*, 2014. 2

[11] M. Fischler and R. Bolles. Random sample consensus: a paradigm for model fitting with applications to image analysis and automated cartography. *CACM*, 24(6):381–395, 1981. 1, 6

[12] R. Girshick. Fast R-CNN. In *ICCV*, 2015. 3

[13] R. Girshick, J. Donahue, T. Darrell, and J. Malik. Rich feature hierarchies for accurate object detection and semantic segmentation. In *CVPR*, 2014. 3

[14] C. Goller and A. Kuchler. Learning task-dependent distributed representations by backpropagation through structure. In *ICNN*, 1996. 3

[15] A. Graves and J. Schmidhuber. Offline handwriting recognition with multidimensional recurrent neural networks. In *NIPS*, 2009. 3

[16] P. Gronat, G. Obozinski, J. Sivic, and T. Pajdla. Learning per-location classifiers for visual place recognition. In *CVPR*, 2013. 2

[17] A. Guzman-Rivera, P. Kohli, B. Glocker, J. Shotton, T. Sharp, A. Fitzgibbon, and S. Izadi. Multi-Output Learning for Camera Relocalization. In *CVPR*, 2014. 2

[18] C. Hazirbas, L. Ma, C. Domokos, and D. Cremers. Fusenet: Incorporating depth into semantic segmentation via fusion-based cnn architecture. In *ACCV*, 2016. 3

[19] K. He, X. Zhang, S. Ren, and J. Sun. Deep residual learning for image recognition. In *CVPR*, 2016. 3

[20] S. Hochreiter and J. Schmidhuber. Long short-term memory. In *NECO*, 1997. 3

[21] A. Kendall and R. Cipolla. Modelling uncertainty in deep learning for camera relocalization. In *ICRA*, 2016. 1, 3, 5, 6

[22] A. Kendall, M. Grimes, and R. Cipolla. Posenet: A convolutional network for real-time 6-dof camera relocalization. In *ICCV*, 2015. 1, 2, 3, 4, 5, 6, 7, 8

[23] D. P. Kingma and J. L. Ba. Adam: A method for stochastic optimization. *ICLR*, 2015. 3, 5

[24] I. Kokkinos. Pushing the boundaries of boundary detection using deep learning. In *ICLR*, 2016. 3

[25] A. Krizhevsky, I. Sutskever, and G. E. Hinton. ImageNet Classification with Deep Convolutional Neural Networks. In *NIPS*, 2012. 3

[26] Z. Kukelova, M. Bujnak, and T. Pajdla. Real-time solution to the absolute pose problem with unknown radial distortion and focal length. In *ICCV*, 2013. 1

[27] B. Li, C. Shen, Y. Dai, A. van den Hengel, and M. He. Depth and surface normal estimation from monocular images using regression on deep features and hierarchical crfs. In *CVPR*, 2015. 3

[28] Y. Li, N. Snavely, D. Huttenlocher, and P. Fua. Worldwide pose estimation using 3d point clouds. In *ECCV*, 2012. 1, 2, 6

[29] Y. Li, N. Snavely, and D. P. Huttenlocher. Location Recognition Using Prioritized Feature Matching. In *ECCV*, 2010. 1, 2, 6

[30] X. Liang, X. Shen, D. Xiang, J. Feng, L. Lin, and S. Yan. Semantic object parsing with local-global long short-term memory. In *CVPR*, 2016. 3, 4

[31] H. Lim, S. N. Sinha, M. F. Cohen, and M. Uyttendaele. Real-time image-based 6-dof localization in large-scale environments. In *CVPR*, 2012. 1

[32] D. Lowe. Distinctive image features from scale-invariant keypoints. *IJCV*, 60(2):91–110, 2004. 1

[33] S. Lynen, T. Sattler, M. Bosse, J. Hesch, M. Pollefeys, and R. Siegwart. Get Out of My Lab: Large-scale, Real-Time Visual-Inertial Localization. In *RSS*, 2015. 1, 2

[34] K. Maninis, J. Pont-Tuset, P. Arbeláez, and L. V. Gool. Convolutional oriented boundaries. In *ECCV*, 2016. 3

[35] H. Noh, S. Hong, and B. Han. Learning deconvolution network for semantic segmentation. *ICCV*, 2015. 3

[36] S. Ren, K. H. and Ross Girshick, and J. Sun. Faster R-CNN: Towards real-time object detection with region proposal networks. In *NIPS*, 2015. 3

[37] O. Russakovsky, J. Deng, H. Su, J. Krause, S. Satheesh, S. Ma, Z. Huang, A. Karpathy, A. Khosla, M. Bernstein, A. C. Berg, and L. Fei-Fei. ImageNet Large Scale Visual Recognition Challenge. *IJCV*, 115(3):211–252, 2015. 3, 4

[38] T. Sattler, M. Havlena, F. Radenović, K. Schindler, and M. Pollefeys. Hyperpoints and Fine Vocabularies for Large-Scale Location Recognition. In *ICCV*, 2015. 2

[39] T. Sattler, M. Havlena, K. Schindler, and M. Pollefeys. Large-Scale Location Recognition And The Geometric Burstiness Problem. In *CVPR*, 2016. 2

[40] T. Sattler, B. Leibe, and L. Kobbelt. Fast image-based localization using direct 2d-to-3d matching. In *ICCV*, 2011. 1

[41] T. Sattler, B. Leibe, and L. Kobbelt. Efficient & Effective Prioritized Matching for Large-Scale Image-Based Localization. *PAMI*, 2016 (to appear). 1, 2, 5, 6, 7, 8

[42] J. L. Schönberger and J.-M. Frahm. Structure-from-motion revisited. In *CVPR*, 2016. 1

[43] J. Shotton, B. Glocker, C. Zach, S. Izadi, A. Criminisi, and A. Fitzgibbon. Scene coordinate regression forests for camera relocalization in rgbd images. *CVPR*, 2013. 2, 4, 5, 6, 7

[44] K. Simonyan and A. Zisserman. Very deep convolutional networks for large-scale image recognition. *ICLR*, 2015. 3

[45] I. Sutskever, O. Vinyals, and Q. V. Le. Sequence to sequence learning with neural networks. In *NIPS*, 2014. 3

[46] L. Svärm, O. Enqvist, F. Kahl, and M. Oskarsson. City-Scale Localization for Cameras with Known Vertical Direction. *PAMI*, 2016 (to appear). 1, 2

- [47] C. Szegedy, W. Liu, Y. Jia, P. Sermanet, S. Reed, D. Anguelov, D. Erhan, V. Vanhoucke, and A. Rabinovich. Going deeper with convolutions. In *CVPR*, 2015. [3](#)
- [48] A. Torii, R. Arandjelović, J. Sivic, M. Okutomi, and T. Pajdla. 24/7 place recognition by view synthesis. In *CVPR*, 2015. [2](#)
- [49] A. Torii, J. Sivic, T. Pajdla, and M. Okutomi. Visual Place Recognition with Repetitive Structures. In *CVPR*, 2013. [2](#)
- [50] J. Valentin, M. Nießner, J. Shotton, A. Fitzgibbon, S. Izadi, and P. Torr. Exploiting Uncertainty in Regression Forests for Accurate Camera Relocalization. In *CVPR*, 2015. [3](#)
- [51] R. R. Varior, B. Shuai, J. Lu, D. Xu, and G. Wang. A siamese long short-term memory architecture for human re-identification. In *ECCV*, 2016. [3](#), [4](#)
- [52] F. Visin, K. Kastner, K. Cho, M. Matteucci, A. Courville, and Y. Bengio. Renet: A recurrent neural network based alternative to convolutional networks. *arXiv:1505.00393*, 2015. [3](#), [4](#)
- [53] T. Weyand, I. Kostrikov, and J. Philbin. Planet - photo geolocation with convolutional neural networks. *ECCV*, 2016. [1](#), [3](#)
- [54] C. Wu. Towards linear-time incremental structure from motion. In *3DV*, 2013. [6](#)
- [55] C. Wu, S. Agarwal, B. Curless, and S. M. Seitz. Multicore Bundle Adjustment. In *CVPR*, 2011. [6](#)
- [56] A. R. Zamir and M. Shah. Accurate image localization based on google maps street view. In *ECCV*, 2010. [2](#)
- [57] A. R. Zamir and M. Shah. Image Geo-Localization Based on Multiple Nearest Neighbor Feature Matching Using Generalized Graphs. *PAMI*, 36(8):1546–1558, 2014. [2](#)
- [58] B. Zeisl, T. Sattler, and M. Pollefeys. Camera pose voting for large-scale image-based localization. In *ICCV*, 2015. [1](#), [2](#)
- [59] W. Zhang and J. Kosecka. Image based localization in urban environments. In *3DPVT*, 2006. [2](#)
- [60] B. Zhou, A. Lapedriza, J. Xiao, A. Torralba, and A. Oliva. Learning deep features for scene recognition using places database. In *NIPS*, 2014. [5](#)